




Article

One-Step Construction of Multi-Walled CNTs Loaded with Alpha-Fe₂O₃ Nanoparticles for Efficient Photocatalytic Properties

Jianle Xu ^{1,2}, Qiang Wen ¹, Xiao Zhang ³, Yinhui Li ¹, Zeyue Cui ¹, Pengwei Li ^{1,*} and Chunxu Pan ²

- ¹ Center of Nano Energy and Devices, College of Information and Computer, Taiyuan University of Technology, Taiyuan 030000, China; xujianle@whu.edu.cn (J.X.); wenqiang@tyut.edu.cn (Q.W.); liyinhui@tyut.edu.cn (Y.L.); cuizheyue@tyut.edu.cn (Z.C.)
- ² School of Physics and Technology, and MOE Key Laboratory of Artificial Micro, and Nano-Structures, Wuhan University, Wuhan 430072, China; cxpan@whu.edu.cn
- ³ College of Environmental Science and Engineering, Taiyuan University of Technology, Taiyuan 030000, China; zhangxiao02@tyut.edu.cn
- * Correspondence: lipengwei@tyut.edu.cn; Tel.: +86-152-3536-4807

Abstract: The aggregation and the rapid restructuring of the photoinduced electron–hole pairs restructuring in the process of photoelectric response remains a great challenge. In this study, a kind of Multi-walled carbon nanotubes loaded Alpha-Fe₂O₃ (CNTs/ α -Fe₂O₃) heterostructure composite is successfully prepared via the one-step method. Due to the synergistic effect in the as-prepared CNTs/ α -Fe₂O₃, the defect sites and oxygen-containing functional groups of CNTs can dramatically improve the interface charge separation efficiency and prevent the aggregation of α -Fe₂O₃. The improved photocurrent and enhanced hole–electron separation rate in the CNTs/ α -Fe₂O₃ is obtained, and the narrower band gap is measured to be 2.8 eV with intensive visible-light absorption performance. Thus, the CNTs/ α -Fe₂O₃ composite serves as an excellent visible light photocatalyst and exhibits an outstanding photocatalytic activity for the cationic dye degradation of rhodamine B (RhB). This research supplies a fresh application area for α -Fe₂O₃ photocatalyst and initiates a new approach for design of high efficiency photocatalytic materials.

Keywords: CNTs; alpha-Fe₂O₃; synergistic effect; heterostructure; photocatalytic properties



Citation: Xu, J.; Wen, Q.; Zhang, X.; Li, Y.; Cui, Z.; Li, P.; Pan, C. One-Step Construction of Multi-Walled CNTs Loaded with Alpha-Fe₂O₃ Nanoparticles for Efficient Photocatalytic Properties. *Materials* **2021**, *14*, 2820. <https://doi.org/10.3390/ma14112820>

Academic Editor: Klára Hernádi

Received: 27 April 2021
Accepted: 24 May 2021
Published: 25 May 2021

Publisher's Note: MDPI stays neutral with regard to jurisdictional claims in published maps and institutional affiliations.



Copyright: © 2021 by the authors. Licensee MDPI, Basel, Switzerland. This article is an open access article distributed under the terms and conditions of the Creative Commons Attribution (CC BY) license (<https://creativecommons.org/licenses/by/4.0/>).

1. Introduction

Currently, environmental pollution has become a potential threat to the sustainable development of human ecology. Utilization of solar energy and photocatalyst degrades organic pollutants and produces hydrogen by water splitting, showing great potential in energy conversion and environmental governance [1–3]. It is important that one of the greatest challenges under the circumstances of the photo-catalysis is how to optimize the efficiency of photo-catalysts to reduce the recombination of photogenerated charge carriers and enhance the absorption intensity and range of excitation light, which will depend on the types and performances (e.g., crystalline structure, width of the band gap, specific surface and so on) of the photocatalyst. Up to now, many efforts have been dedicated to searching for high photocatalytic activity materials such as n-type semiconductor materials TiO₂ [4], ZnO [5], SnO₂ [6], Fe₂O₃ [7], etc. A great deal of work has been done on the preparation of pure α -Fe₂O₃ for photocatalysis, such as the use of ultrasonic-assisted method [8], etc. Compared with other preparation methods, the one-step synthesis method has significant advantages, as the experimental operation is simple and feasible, and the synthesized nanoparticles have small particle size and good dispersion.

Nano iron oxides are widely used in heterogeneous catalyst, and alpha-iron oxide (α -Fe₂O₃) has been considered as one of the significant members in the energy conversion field due to its favorable band gap, stability, and abundance. By its narrow band gap

and high stability, it absorbs visible light and other sources. However, as α -Fe₂O₃ has denied electron-hole pair recombination [9,10], the rapid reorganization recombination of the photoinduced electron–hole pairs reduces photocatalytic performance expressly, and the photocatalytic reaction is slightly affected [11,12].

It is well known that making full use of photogenerated carriers is pivotal to improving the activity of photocatalyst based on semiconductor photocatalytic mechanism. Recently, several strategies have been studied extensively, showing that the recombination of the photo-generated electrons and holes is able to be restrained by constructing of heterojunction [13,14], development of Z-scheme heterojunction [15,16] and coupling of support materials [17–19]. Combining of carbon-based materials (e.g., activated carbon, graphene, carbon quantum dots, CNTs) for catalyst has attracted much attention as new-fire strategy to transfer of photoinduced charge carriers and increase lifetime during the photocatalytic activity. There have been many reports on the synthesis of CNTs/ α -Fe₂O₃ nanocomposite [20]. According to a recent study, CNTs have increased the photocatalytic performance because of excellent electron transport capability and enhanced separation rate of charge carriers [21–25]. Moreover, the oxygen-containing functional groups and defect sites on the outside of carbon materials can also effectively inhibit the agglomeration of semiconductor nanoparticles (NPs) [26,27]. To the best of our knowledge, heterostructure hybrids designed based on Multi-walled CNTs and α -Fe₂O₃ for photocatalytic have rarely been reported. Moreover, limited progress has been made towards a basic understanding of photocatalytic mechanism in α -Fe₂O₃ heterostructure materials. Thus, designing α -Fe₂O₃@carbon-based materials (e.g., activated carbon, graphene, carbon quantum dots, and CNTs) will be an effective pathway to improving photochemical and catalytic properties [21].

Herein, we reported a novel and simple strategy to solve the aforementioned defect of the α -Fe₂O₃ in photocatalytic filed. The CNTs/ α -Fe₂O₃ composite has been synthesized by a one-step hydrothermal method successfully. This work demonstrates that CNTs/ α -Fe₂O₃ composite exhibits greatly improved photocatalytic activity on the degradation of RhB attributed to improved photocurrent and enhanced hole–electron separation rate, when compared to single α -Fe₂O₃. Meanwhile, this facile method for novel heterojunction photocatalysts may be widely used in the field of water treatment.

2. Materials and Methods

2.1. Materials

Multi-walled CNTs, with size 0.5–2 μ m in length and 30–50 nm in diameter, were purchased from the Chinese Academy of Science, Chengdu Organic Chemistry Co., Ltd., Chengdu, China, Ferric chloride hexahydrate (FeCl₃·6H₂O, 99%), phenol (C₆H₆O, 99.5%), sodium acetate (CH₃COONa, 99%), rhodamine B (C₂₈H₃₁ClN₂O₃, RhB), methyl orange (C₁₄H₁₄N₃SO₃Na, MO), congo red (C₃₂H₂₂N₆Na₂O₆S₂, CR), and methylene blue (C₁₆H₁₈ClN₃S, MB) were from Sinopharm Chemical Reagent Co., Ltd. (Taiyuan, China). No further purification was done before the use of all the reagents and chemicals.

2.2. Synthesis of α -Fe₂O₃ Nanoparticles

The α -Fe₂O₃ NPs were prepared using a method reported by our previous work [9]. 0.02 M FeCl₃·6H₂O and 0.1 M CH₃COONa was dispersed into 60 mL deionized water. Then, the suspension was transferred and sealed in a stainless-steel autoclave with 250 °C for 5 h. Lastly, the obtained sample was dried in vacuum oven at 60 °C.

2.3. Synthesis of CNTs/ α -Fe₂O₃ Composite Nanomaterials

The CNTs/ α -Fe₂O₃ composite was prepared via the one-step hydrothermal process. Firstly, 0.324 g of FeCl₃·6H₂O and 0.492 g CH₃COONa was dispersed into 30 mL deionized water. After that, CNTs with different content (2.5%, 5%, 7.5%) were added into the above solution. After ultrasonic process for 30 min, the mixed sample was transferred into a stainless-steel autoclave, which was kept at 250 °C for 5 h. After the reaction, the product was harvested through several rinse–precipitation cycles with deionized water and ethanol

and dried at 60 °C over-night. The CNTs/ α -Fe₂O₃ composites finally were obtained. The obtained products (CNTs-loaded with α -Fe₂O₃NPs) corresponding to proportion of CNTs addition (2.5%, 5%, 7.5%) were denoted as CNTs/ α -Fe₂O₃: S₁-S₃, respectively.

2.4. Characterization

The structure of samples was measured by X-ray diffraction (XRD) patterns which were provided by a powder diffractometer (Bruker AXS, Karlsruhe, Germany). The structure and morphology were measured by scanning electron microscopy (SEM, JSM-7001F, JEOL, Tokyo, Japan) and transmission electron microscopy (TEM, 2100F, JEOL, Tokyo, Japan). Energy-dispersive X-ray analysis (EDX, INCA Penta FETx3) was provided with the SEM. Raman spectra were measured by the spectrometer (LabRAM HR 800UV, HPRIBA JOBIN YVON, Paris, France). UV-VIS spectra were measured using the spectrophotometer (3100 UV-VIS-NIR, Shimadzu, Kyoto, Japan).

2.5. Photoelectrochemical Performance of α -Fe₂O₃ and CNTs/ α -Fe₂O₃

The photoelectrochemical (PEC) is measured by an electrochemical workstation (IM6, Zahner, Karlsruhe, Germany) with a 500 W Xe light furnished with a cut-off filter ($\lambda > 420$ nm) used for the source of visible light. A saturated Ag/AgCl and Pt wire was used as a counter and a reference electrode, indium-tin oxide (ITO) glass, as working electrode. Then, 1 mg CNTs/ α -Fe₂O₃, 5 wt.% Nafion (10 mL), ethanol (0.2 mL), and water (0.2 mL) were mixed to form a suspension. After ultrasonication for 30 min, the suspension was coated on the surface of ITO glasses (2.0 cm \times 2.0 cm) and dried at 60 °C for several hours to prepare the photoelectrodes. In the PEC measurements, Na₂SO₄ (0.5 M) was adopted as the electrolyte. The photocurrent properties of the photoanode were evaluated by chronoamperometric I-t curves measured with interval time of 60 s.

For the test of photocatalytic performance, photocatalyst (5 mg) was dissolved into Phenol, RhB MB, MO (50 mL), and CR (0.01 mM), respectively, in order to produce the suspension by magnetically stirring continually in a dark environment for 1 h to reach adsorption-desorption equilibrium. After that, the 0.3 mL of hydrogen peroxide solution (H₂O₂, 30 wt.%) was added into above suspension with a refrigerating plant under magnetic stirring, and the vertical distance between the lamps was 50 cm (the energy directly radiated was about 95 mW/mL). During the experiment, every 30 min, 3 mL of solution was extracted from the suspension, and the change of the maximum absorbance was measured by spectrophotometer, while the concentration of dye in the filtrate at different intervals was measured.

3. Results and Discussion

Figure 1 shows that structure and composition characterization of CNTs/ α -Fe₂O₃ composite highly regular α -Fe₂O₃ NPs grow on the CNTs. The morphology of microstructures of the CNTs and CNTs/ α -Fe₂O₃ were investigated by SEM, as shown in Figure 1a,b. One could find that a large number of α -Fe₂O₃ NPs adhere to the surface of CNTs. As shown in Figure 1c,d, the detailed microstructures of the CNTs/ α -Fe₂O₃ composite was conducted by low-magnification TEM and high-resolution TEM. Significantly, the α -Fe₂O₃ NPs on the surface of CNTs can be observed clearly. Moreover, one can find that α -Fe₂O₃ with an average diameter of 20–30 nm was uniformly deposited on the outside of CNTs after a hydrothermal process. The average diameter of the CNTs was 30–50 nm, and the length was about 1–2 μ m. As shown in Figure 1d, the clear HRTEM image observations reveal that the CNTs/ α -Fe₂O₃ heterostructure nanocrystals are composed of CNTs and α -Fe₂O₃ NPs. Furthermore, HRTEM image of the typical hybrid nanostructure exhibits a single-crystalline structure with the spacing of 0.27 nm, corresponding to the {110} planes of α -Fe₂O₃ [28], and the interlayer spacing of graphite in Multi-walled CNTs is 0.34 nm [29]. No other contaminations are observed, possibly indicating that their interface between the CNTs and α -Fe₂O₃ NPs is “clean”.

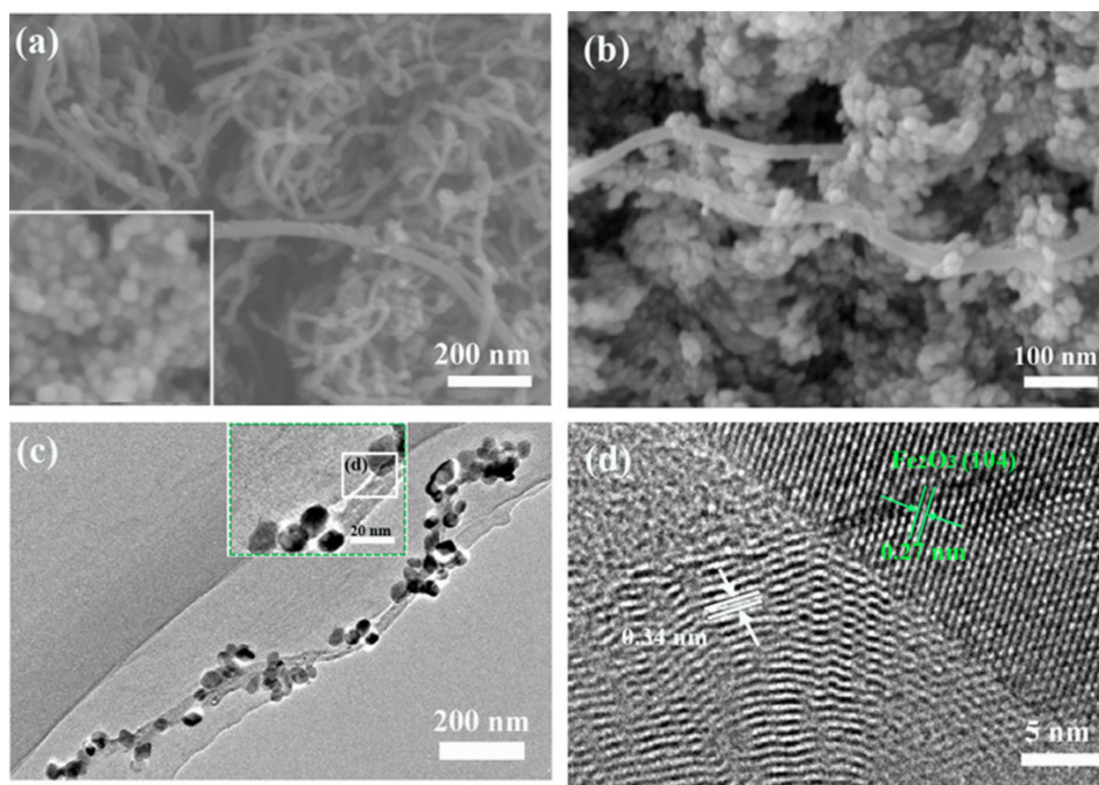


Figure 1. (a) SEM image of CNTs and pure α -Fe₂O₃ (inset); (b) CNTs/ α -Fe₂O₃ NPs; (c) TEM image of CNTs/ α -Fe₂O₃ nanocomposite (inset); (d) HRTEM image of CNTs/ α -Fe₂O₃.

Figure 2a shows XRD spectra of the single CNTs, α -Fe₂O₃ and CNTs/ α -Fe₂O₃-S_x composite. All the diffraction peaks are indexed by the rhombohedral α -Fe₂O₃ phase (JCPDS card No. 33-0664) without any peaks of other phases, which indicates the enhanced purity of as-prepared α -Fe₂O₃. The XRD pattern of the CNTs/ α -Fe₂O₃ composite has a similar diffraction to α -Fe₂O₃. However, unobserved CNTs signal in the XRD pattern indicates the amount of CNTs in the sample was very low and the loading content of CNTs didn't affect the crystal structure of α -Fe₂O₃ [30]. More composition information can be confirmed by the Raman spectra, the Raman spectra of α -Fe₂O₃ [31], CNTs and CNTs/ α -Fe₂O₃-S_x in a range of 800–1800 cm⁻¹ as shown in Figure 2b. Raman spectrum of CNTs/ α -Fe₂O₃-S_x with two peaks at 1330 and 1585 cm⁻¹ assigned to D and G bands confirms the presence of CNTs in the nanocomposite [32]. D and G bands arise from the defects and disorder in carbon materials and stretching mode of C-C bonds in the graphite crystallites, respectively [33,34]. For pure CNTs, the I_D/I_G value is 1.23. In the presence of α -Fe₂O₃, the graphitization degree of CNTs was improved, and the I_D/I_G value is about 1.1. Based on the above analysis, the assumption that the amount of CNTs in the sample was very low proved to be correct.

The photoelectrochemical (PEC) performance of α -Fe₂O₃ with different loading amounts of CNTs can account for the photocatalytic activity (Figure 3a). With the periodic visible light irradiation at 60 s intervals in a conventional three-electrode system, the transient photocurrent values of the work electrodes were measured. The photocurrent density of CNTs/ α -Fe₂O₃-S₂ reached 0.34 mA/cm² and was about 2.8 times as high as that of pure α -Fe₂O₃. This superior performance could be attributed to the introduction of CNTs, leading to the formation of synergistic effect. This synergistic effect makes it easier for CNTs to capture charge and improves photoelectron generation [35,36]. However, the photocurrent density of the composite decreases again, with a high CNTs loading (beyond 5wt% of CNTs/ α -Fe₂O₃). This inhibitory effect may be associated with the balance of synergistic between CNTs and α -Fe₂O₃ [19,37]. The optical performance and photo absorption

capacity of as-prepared nanocomposite were evaluated by the UV–S diffuse reflectance spectra. The visible light source is a 500W Xe (the wavelength distributes from 400 to 800 nm) light furnished ($\lambda > 420$ nm). In addition, the measured power of visible light irradiation on the sample is about 95 mW/mL. Here, pure α -Fe₂O₃ and CNTs/ α -Fe₂O₃-S₂ are assumed to be a direct band gap semiconductor [21]. There is a close relationship between the band gap energies (E_g) of absorbed wavelength range and semiconductors. The value of E_g are calculated by Kubelka–Munk. Figure 3b clearly displays the visual absorption peak of the single α -Fe₂O₃ at corresponding to band gap energy of 2.37 eV (Figure 3c). However, the absorption peak of typical CNTs/ α -Fe₂O₃-S₂ has about 23 nm red shift, which is 457 nm. The band gap energy of typical CNTs/ α -Fe₂O₃-S₂ is 2.08 eV which is smaller than that of pure α -Fe₂O₃. The course of band gap narrowing in CNTs/ α -Fe₂O₃ is the surface defects formed of CNTs [38,39]. Obviously, the introduction of CNTs directly exhibits positive and improved impact on the photocatalytic properties and solar energy efficient utilization.

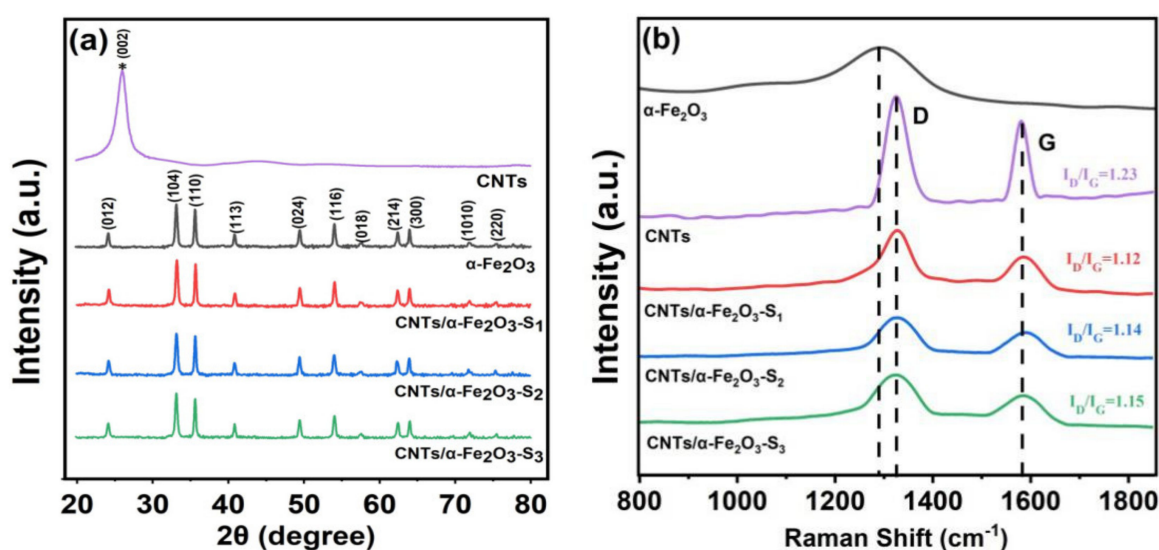


Figure 2. (a,b) XRD pattern and Raman spectra of CNTs, α -Fe₂O₃, and CNTs/ α -Fe₂O₃-S_x composite S1, S2, and S3 are α -Fe₂O₃ with different mass ratio of CNTs loaded (2.5%, 5% and 7.5%).

The photocatalytic activities of CNTs/ α -Fe₂O₃ were measured by the degradation of RhB under visible light irradiation in aqueous solution. The dye concentration was analyzed by measuring the absorption intensity of RhB at 554 nm. With the extension of irradiation time, the coloration and absorption peak intensity of RhB solution decreased gradually, which means the concentration of RhB is continuously reduced. Figure 4a,b shows the variation of the RhB relative concentrations (C_t/C_0 , and $-\ln(C_t/C_0)$) as a function of irradiation time, where C_t is the RhB concentration of the irradiation time and C_0 is the initial concentration. Here, the main purpose of adding H₂O₂ is to make the whole reaction system in the Fenton system, Fe₂O₃ and H₂O₂, through Fenton reaction to generate strong oxidizing groups such as OH. In the presence of these strong oxidizing groups, the dye can be degraded. After irradiation for 5 h, only the photodegradation of RhB with H₂O₂ shows that the self-degradation can almost inappreciable, and 53%, 70.1%, and 49% RhB were degraded in the presence of CNTs/ α -Fe₂O₃-S₁, CNTs/ α -Fe₂O₃-S₂, CNTs/ α -Fe₂O₃-S₃, while there were degradation degrees of 46% and 9.1% by using the pure α -Fe₂O₃ and H₂O₂. Figure 4b indicates that the degradation rate constant of CNTs/ α -Fe₂O₃-S₂ reaches the maximum of 0.219/h. Obviously, when CNTs were loaded into α -Fe₂O₃, the photocatalytic of the prepared CNTs/ α -Fe₂O₃-S_x samples had a prominent enhancement, especially with the loaded weight ratio of 5% (CNTs/ α -Fe₂O₃-S₂). This could be ascribed to the loading of CNTs prolonging the recombination time of electron-hole pairs [39]. For CNTs/ α -Fe₂O₃, carriers can transfer from α -Fe₂O₃ to CNTs through

the interface easily due to the defects of CNTs [25,40]. In cycle test experiments, samples were collected by centrifugation and washed before each test to ensure the purity. The RhB degradation ratio remained near 70% after 5 cycles (Figure 4c), indicating its excellent stability and photoactivity.

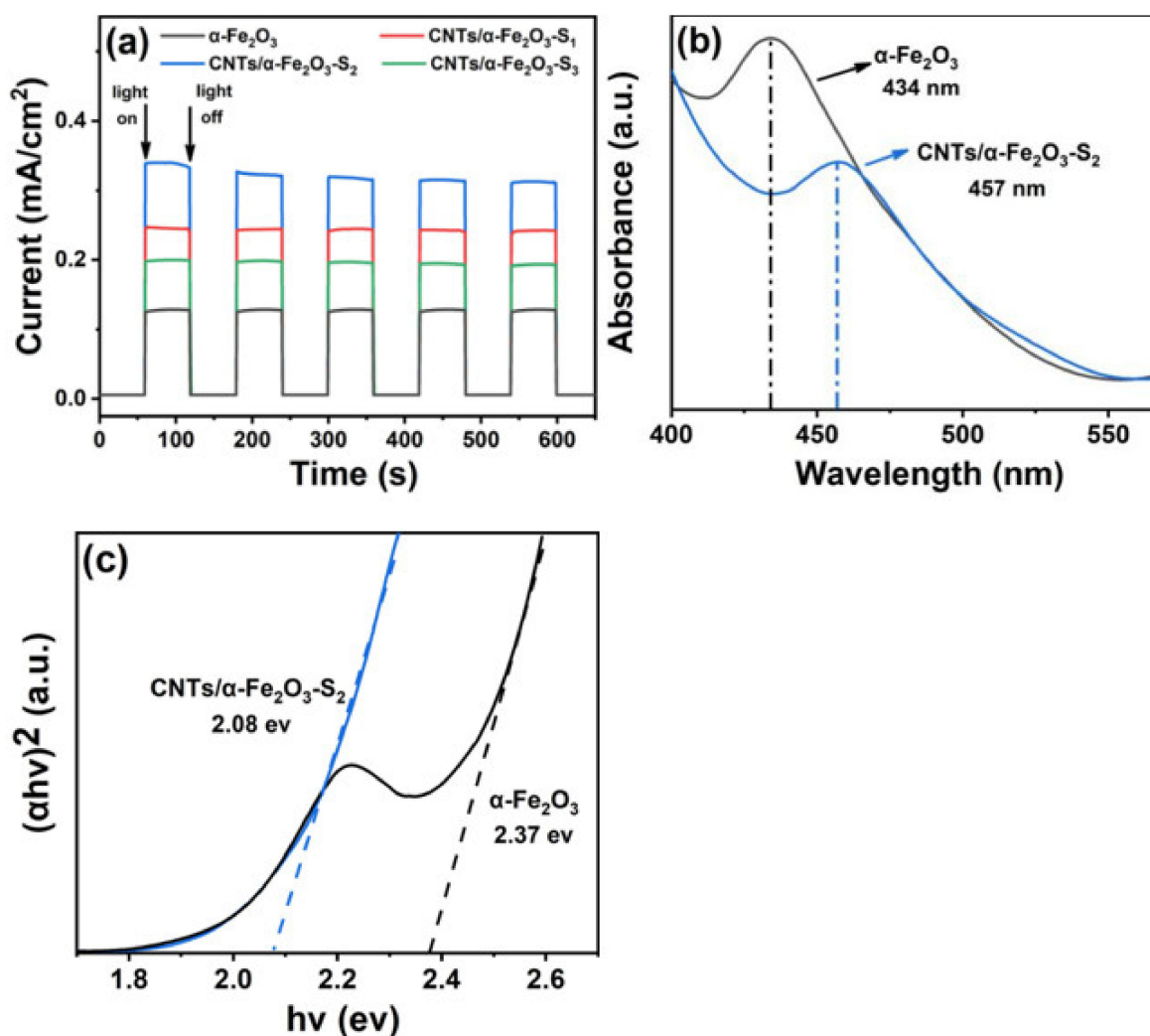


Figure 3. (a) Photocurrent density of $\alpha\text{-Fe}_2\text{O}_3$ and CNTs/ $\alpha\text{-Fe}_2\text{O}_3\text{-S}_x$; (b) UV-VIS absorption spectra for $\alpha\text{-Fe}_2\text{O}_3$ and CNTs/ $\alpha\text{-Fe}_2\text{O}_3\text{-S}_2$; (c) linear fits (dashed lines) of the $(\alpha h\nu)^2$ curves.

The photocatalytic activities of samples can be further evaluated by the degradation of dyes phenol, MB, MO, and CR. Figure 5 plots the comparison of photodegradation of different kinds of dyes. The degradation rate of CNTs/ $\alpha\text{-Fe}_2\text{O}_3\text{-S}_2$ to cationic dye RhB, MB, neutral dye phenol (in the middle of the bar), and anionic dyes MO and CR were 70.1%, 60.2%, 41.2%, 31.8%, and 15.7%, respectively, which illustrates CNTs/ $\alpha\text{-Fe}_2\text{O}_3$ has a prominent photocatalytic performance in the cationic dyes [10].

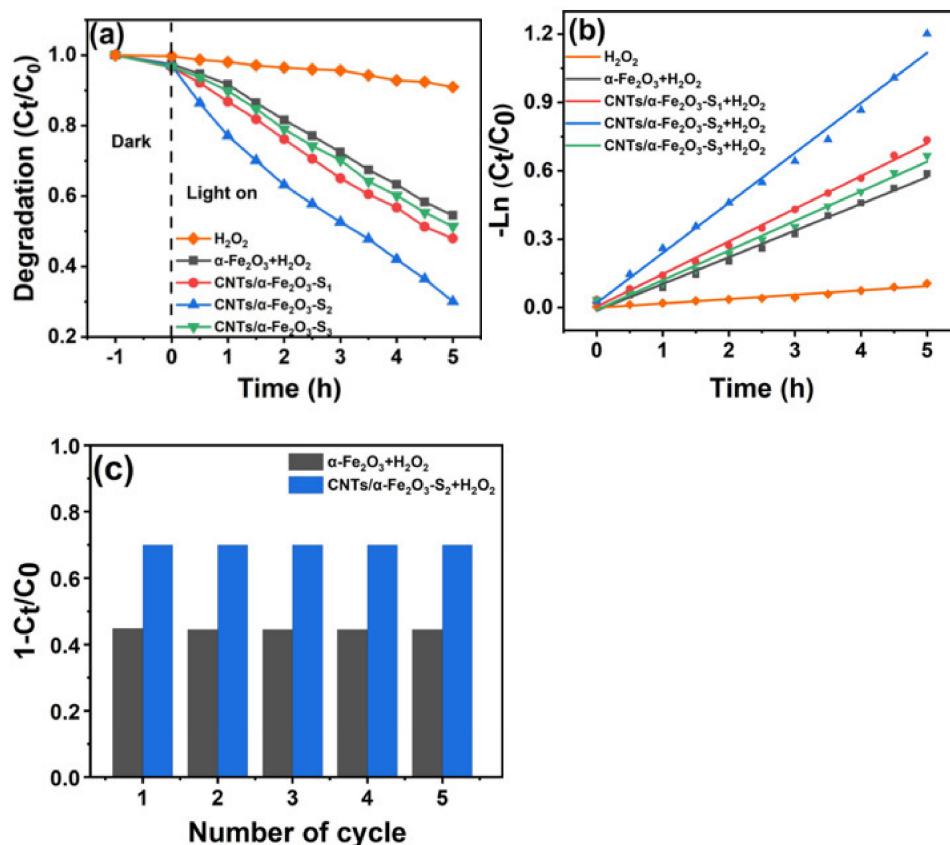


Figure 4. (a) Photocatalytic degradation of RhB with different samples; (b) kinetic curves of the RhB degradation; (c) cycle degradation of RhB.

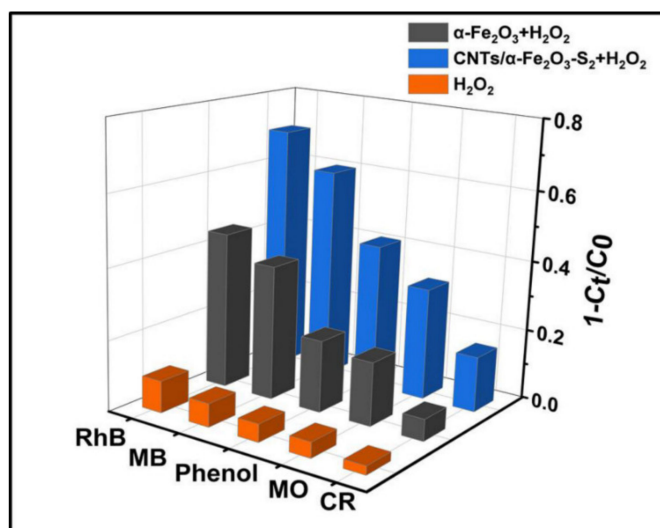


Figure 5. Photocatalytic degradation of several different pollutants with prepared photocatalysts.

In Figure 6, the mechanism of enhancing photocatalytic performance by CNTs loaded α-Fe₂O₃ was proposed based on the mentioned above analysis. Under the irradiation of sunlight, electrons from the valence band (VB) of the semiconductor are motivated into its conduction band (CB), meanwhile creating electron hole in the VB [10]. First, photoexcited electrons and the holes are rapidly recombined; then, only a few of the electrons and holes are involved in the reaction, which can be used to degrade pollutants. Secondly, when CNTs were loaded into α-Fe₂O₃, the free electrons can transfer from α-Fe₂O₃ to CNTs through the interface between them more easily due to the defects of CNTs, leading to

a higher hole-electron separation rate [41–43]. Then, more carriers can be transferred to the active site to participate in the photocatalytic process, greatly reducing the electron-hole recombination process in $\alpha\text{-Fe}_2\text{O}_3$. In conclusion, the main reaction process can be expressed as follows:

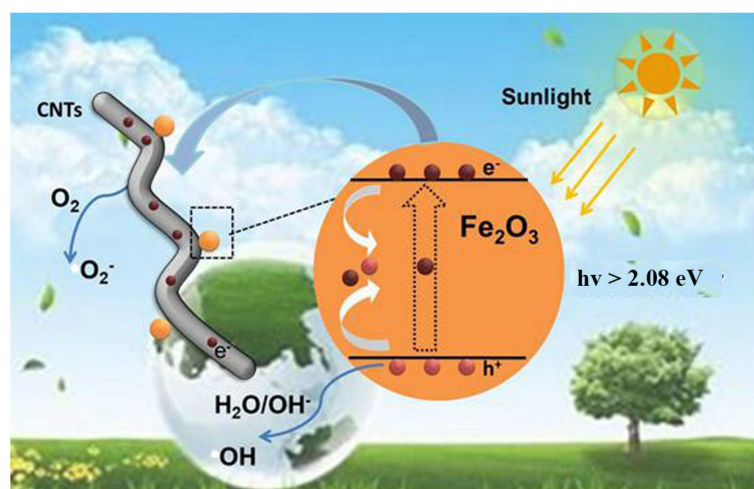
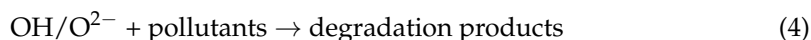
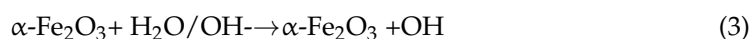
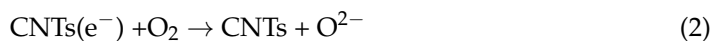
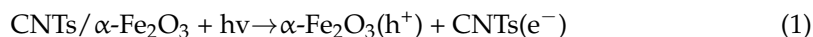


Figure 6. Schematic illustration of proposed photocatalytic mechanism for CNTs/ $\alpha\text{-Fe}_2\text{O}_3$.

4. Conclusions

In the present research, CNTs/ $\alpha\text{-Fe}_2\text{O}_3$ nanocomposite was synthesized via a simple one-step hydrothermal method. The as-prepared CNTs/ $\alpha\text{-Fe}_2\text{O}_3$ composites possessed a heterojunction structure, where the $\alpha\text{-Fe}_2\text{O}_3$ NPs were grown in the surface of Multi-walled carbon nanotubes. Because of the special structure of the composites, the high times photocurrent output value, and under visible light irradiation, the narrower band gap (2.08 eV) and improved photocatalytic properties for the degradation of RhB dye, the obtained CNTs/ $\alpha\text{-Fe}_2\text{O}_3$ exhibited excellent photocatalytic performance. Thanks to the introduction of CNTs, the separation of photogenerated carriers is promoted. Taking advantage of this feature, introducing a certain quality ratio of CNTs into $\alpha\text{-Fe}_2\text{O}_3$ can highly perfect the photocatalytic properties. The results of our experiments indicate that CNTs/ $\alpha\text{-Fe}_2\text{O}_3$ composites may be a promising photocatalyst to reduce the cost of the water treatment process.

Author Contributions: Conceptualization, J.X. and P.L.; methodology, Q.W. and J.X.; investigation, X.Z. and J.X.; data curation, C.P., Z.C., P.L., Q.W., Y.L. and J.X.; writing—original draft preparation, Q.W. and J.X.; writing—review and editing, P.L. and J.X.; supervision, C.P.; funding acquisition, P.L. All authors have read and agreed to the published version of the manuscript.

Funding: This work was supported by the National Natural Science Foundation of China (Grant Nos. 11602159, 51205276, and 61474079) and the Special Talents in Shanxi Province (Grant No. 201901D211074).

Institutional Review Board Statement: Not applicable.

Informed Consent Statement: Not applicable.

Data Availability Statement: Data is contained within the article.

Conflicts of Interest: The authors declare no conflict of interest.

References

1. Yang, J.; Cooper, J.K.; Toma, F.M.; Walczak, K.A.; Favaro, M.; Beeman, J.W.; Favaro, M.; Beeman, J.W.; Hess, L.H.; Wang, C.; et al. A multifunctional biphasic water splitting catalyst tailored for integration with high-performance semiconductor photoanodes. *Nat. Mater.* **2017**, *16*, 335–341. [[CrossRef](#)]
2. He, K.; Chen, G.; Zeng, G.; Chen, A.; Huang, Z.; Shi, J.; Huang, T.; Peng, M.; Hu, L. Three-dimensional graphene supported catalysts for organic dyes degradation. *Appl. Catal. B Environ.* **2018**, *228*, 19–28. [[CrossRef](#)]
3. Pavithra, K.G.; Kumar, P.S.; Jaikumar, V.; Rajan, P.S. Removal of colorants from wastewater: A review on sources and treatment strategies. *J. Ind. Eng. Chem.* **2019**, *75*, 1–19. [[CrossRef](#)]
4. Ge, M.; Cao, C.; Huang, C.; Li, S.; Chen, Z.; Zhang, K.Q.; Deyab, S.S.; Lai, Y. A review of one-dimensional TiO₂ nanostructured materials for environmental and energy applications. *J. Mater. Chem. A* **2016**, *4*, 6772–6801. [[CrossRef](#)]
5. Ong, C.B.; Ng, L.Y.; Mohammad, A.W. A review of ZnO nanoparticles as solar photocatalysts: Synthesis, mechanisms and applications. *Renew. Sustain. Energy Rev.* **2018**, *81*, 536–551. [[CrossRef](#)]
6. Zhang, L.; Yu, W.; Han, C.; Guo, J.; Zhang, Q.; Xie, H.; Shao, Q.; Sun, Z.; Guo, Z. Large scaled synthesis of heterostructured electrospun TiO₂/SnO₂ nanofibers with an enhanced photocatalytic activity. *J. Electrochem. Soc.* **2017**, *164*, 651–656. [[CrossRef](#)]
7. Li, J.; Pei, Q.; Wang, R.; Zhou, Y.; Zhang, Z.; Cao, Q.; Wang, D.; Mi, W.; Du, Y. Enhanced photocatalytic performance through magnetic field boosting carrier transport. *ACS Nano* **2018**, *12*, 3351–3359. [[CrossRef](#)]
8. Zhang, H.L.; Zhu, C.X.; Cao, J.L.; Tang, Q.J.; Li, M.; Kang, P.; Shi, C.L.; Ma, M.J. Ultrasonic-Assisted Synthesis of 2D α -Fe₂O₃@g-C₃N₄ Composite with Excellent Visible Light Photocatalytic Activity. *Catalysts* **2018**, *8*, 457. [[CrossRef](#)]
9. Mishra, M.; Chun, D.M. α -Fe₂O₃ as a photocatalytic material: A review. *Appl. Catal. A Gen.* **2015**, *498*, 126–141. [[CrossRef](#)]
10. Li, D.D.; Yan, X.L.; Yang, M.M.; Luo, C.X.; Li, P.W.; Hu, J.; Li, G.; Jiang, H.B.; Zhang, W.D. 4-Mercaptobenzoic acid assisted synthesis of Au-decorated alpha-Fe₂O₃ nanoparticles with highly enhanced photocatalytic performance. *J. Alloys Compd.* **2016**, *775*, 150–157. [[CrossRef](#)]
11. Ren, L.; Zhou, W.; Sun, B.; Li, H.; Qiao, P.; Xu, Y.; Wu, J.; Lin, K.; Fu, H. Defects-engineering of magnetic γ -Fe₂O₃ ultrathin nanosheets/mesoporous black TiO₂ hollow sphere heterojunctions for efficient charge separation and the solar-driven photocatalytic mechanism of tetracycline degradation. *Appl. Catal. B Environ.* **2019**, *240*, 319–328. [[CrossRef](#)]
12. Singh, J.; Basu, S. Synthesis of mesoporous magnetic Fe₂O₃/g-C₃N₄ monoliths for Rhodamine B removal. *Microporous Mesoporous Mater.* **2020**, *303*, 110299. [[CrossRef](#)]
13. Mou, H.; Wang, J.; Zhang, D.; Yu, D.; Chen, W.; Wang, D.; Mu, T. A one-step deep eutectic solvent assisted synthesis of carbon nitride/metal oxide composites for photocatalytic nitrogen fixation. *J. Mater. Chem. A* **2019**, *7*, 5719–5725. [[CrossRef](#)]
14. Pan, J.; Dong, Z.; Wang, B.; Jiang, Z.; Zhao, C.; Wang, J.; Song, C.; Zheng, Y.; Li, C. The enhancement of photocatalytic hydrogen production via Ti³⁺ self-doping black TiO₂/g-C₃N₄ hollow core-shell nano-heterojunction. *Appl. Catal. B Environ.* **2019**, *242*, 92–99. [[CrossRef](#)]
15. Pan, L.; Cao, S.; Liu, R.; Chen, H.; Jiang, F.; Wang, X. Graphitic carbon nitride grown in situ on aldehyde-functionalized alpha-Fe₂O₃: All-solid-state Z-scheme heterojunction for remarkable improvement of photo-oxidation activity. *J. Colloid Interface Sci.* **2019**, *548*, 284–292. [[CrossRef](#)]
16. Huo, Q.; Qi, X.; Li, J.; Liu, G.; Ning, Y.; Zhang, X.; Zhang, B.; Fu, Y.; Liu, S. Preparation of a direct Z-scheme α -Fe₂O₃/MIL-101(Cr) hybrid for degradation of carbamazepine under visible light irradiation. *Appl. Catal. B Environ.* **2019**, *255*, 117751. [[CrossRef](#)]
17. Sharma, S.; Dutta, V.; Singh, P.; Raizada, P.; Rahmani-Sani, A.; Hosseini-Bandegharai, A.; Thakur, V.K. Carbon quantum dot supported semiconductor photocatalysts for efficient degradation of organic pollutants in water: A review. *J. Clean. Prod.* **2019**, *228*, 755–769. [[CrossRef](#)]
18. Tan, H.L.; Du, A.; Amal, R.; Ng, Y.H. Decorating platinum on nitrogen-doped graphene sheets: Control of the platinum particle size distribution for improved photocatalytic H₂ generation. *Chem. Eng. Sci.* **2019**, *194*, 85–93. [[CrossRef](#)]
19. Zhang, J.J.; Qi, P.; Li, J.; Zheng, X.C.; Liu, P.; Guan, X.X.; Zheng, G.P. Three-dimensional Fe₂O₃-TiO₂-graphene aerogel nanocomposites with enhanced adsorption and visible light-driven photocatalytic performance in the removal of RhB dyes. *J. Ind. Eng. Chem.* **2018**, *61*, 407–415. [[CrossRef](#)]
20. Zhao, Z.; Zhou, X.W.; Zhu, L. Synthesis of Nanosphere α -Fe₂O₃/MWCNT composite as Photo-catalyst for the Degradation of Rhodamine B. In Proceedings of the 4th International Conference on Mechatronics, Materials, Chemistry and Computer Engineering, Xi'an, China, 12–13 December 2015; Volume 39, pp. 2317–2321.
21. Liu, Y.; Jin, W.; Zhao, Y.; Zhang, G.; Zhang, W. Enhanced catalytic degradation of methylene blue by α -Fe₂O₃/graphene oxide via heterogeneous photo-Fenton reactions. *Appl. Catal. B Environ.* **2017**, *206*, 642–652. [[CrossRef](#)]
22. She, X.; Wu, J.; Xu, H.; Mo, Z.; Lian, J.; Song, Y.; Liu, L.; Du, D.; Li, H. Enhancing charge density and steering charge unidirectional flow in 2D non-metallic semiconductor-CNTs-metal coupled photocatalyst for solar energy conversion. *Appl. Catal. B Environ.* **2017**, *202*, 112–117. [[CrossRef](#)]
23. Bellamkonda, S.; Thangavel, N.; Hafeez, H.Y.; Neppolian, B.; Ranga, G. Highly active and stable multi-walled carbon nanotubes-graphene-TiO₂ nanohybrid: An efficient non-noble metal photocatalyst for water splitting. *Catal. Today* **2019**, *321*, 120–127. [[CrossRef](#)]
24. Zhao, S.; Guo, T.; Li, X.; Xu, T.; Yang, B.; Zhao, X. Carbon nanotubes covalent combined with graphitic carbon nitride for photocatalytic hydrogen peroxide production under visible light. *Appl. Catal. B Environ.* **2018**, *224*, 725–732. [[CrossRef](#)]

25. Christoforidis, K.C.; Syrgiannis, Z.; Parola, V.; Montini, T.; Petit, C.; Stathatos, E.; Godin, R.; Durrant, J.R.; Prato, M.; Fornasiero, P. Metal-free dual-phase full organic carbon nanotubes/g-C₃N₄ heteroarchitectures for photocatalytic hydrogen production. *Nano Energy* **2018**, *50*, 468–478. [[CrossRef](#)]
26. Mallakpour, S.; Khadem, E. Carbon nanotube–metal oxide nanocomposites: Fabrication, properties and applications. *Chem. Eng. J.* **2016**, *302*, 344–367. [[CrossRef](#)]
27. Schroeder, V.; Savagatrup, S.; He, M.; Lin, S.; Swager, T.M. Carbon nanotube chemical sensors. *Chem. Rev.* **2019**, *119*, 599–663. [[CrossRef](#)]
28. Wang, X.; Wang, J.; Cui, Z.; Wang, S.; Cao, M. Facet effect of α -Fe₂O₃ crystals on photocatalytic performance in the photo-Fenton reaction. *RSC Adv.* **2014**, *4*, 34387.
29. Kharissova, O.V.; Kharisov, B.I. Variations of interlayer spacing in carbon nanotubes. *RSC Adv.* **2014**, *4*, 30807–30815. [[CrossRef](#)]
30. Li, L.; Li, Z.; Fu, W.; Li, F.; Wang, J.; Wang, W. α -Fe₂O₃@C nanorings as anode materials for high performance lithium ion batteries. *J. Alloys Compd.* **2015**, *647*, 105–109. [[CrossRef](#)]
31. Jansi, B.; Ravi, G.; Yuvakkumar, R.; Ravichandran, S.; Ameen, F.; AlNadhary, S. Sn doped α -Fe₂O₃ (Sn = 0,10,20,30.wt%) photoanodes for photoelectrochemical water splitting applications. *Renew. Energy* **2019**, *133*, 566–574. [[CrossRef](#)]
32. Azzam, E.M.S.; Fathy, A.; Khouly, S.M.; Sami, R.M. Enhancement the photocatalytic degradation of methylene blue dye using fabricated CNTs/TiO₂/AgNPs/Surfactant nanocomposites. *J. Water Process Eng.* **2019**, *28*, 311–321. [[CrossRef](#)]
33. Zhou, N.; An, Q.; Xiao, Z.; Zhai, S.; Shi, Z. Solvothermal synthesis of three-dimensional, Fe₂O₃ NPs-embedded CNT/N-doped graphene composites with excellent microwave absorption performance. *RSC Adv.* **2017**, *7*, 45156–45169. [[CrossRef](#)]
34. Chernyak, S.A.; Ivanov, A.S.; Maslakov, K.I.; Egorov, A.V.; Shen, Z.; Savilov, S.S.; Lunin, V.V. Oxidation, defunctionalization and catalyst life cycle of carbon nanotubes: A Raman spectroscopy view. *Phys. Chem. Chem. Phys.* **2017**, *19*, 2276–2285. [[CrossRef](#)] [[PubMed](#)]
35. Wu, Y.; Ward, B.J.; Li, D.; Zhang, S.; Shi, J.; Jiang, Z. g-C₃N₄@ α -Fe₂O₃/C Photocatalysts: Synergistically Intensified Charge Generation and Charge Transfer for NADH Regeneration. *ACS Catal.* **2018**, *8*, 5664–5674. [[CrossRef](#)]
36. Hassanzadeh, S.A.; Nguyen, C.C.; Do, T.O. Synthesis of Fe₂O₃/Pt/Au nanocomposite immobilized on g-C₃N₄ for localized plasmon photocatalytic hydrogen evolution. *Appl. Surf. Sci.* **2019**, *489*, 741–754. [[CrossRef](#)]
37. Ahmad, A.; Razali, M.H.; Mamat, M.; Mehamod, F.S.B.; Anuar, K. Adsorption of methyl orange by synthesized and functionalized-CNTs with 3-aminopropyltriethoxysilane loaded TiO₂ nanocomposites. *Chemosphere* **2017**, *168*, 474–482. [[CrossRef](#)]
38. Kumar, K.V.A.; Chandana, L.; Ghosal, P.; Subrahmanyam, C. Simultaneous photocatalytic degradation of p-cresol and Cr (VI) by metal oxides supported reduced graphene oxide. *Mol. Catal.* **2018**, *451*, 87–95. [[CrossRef](#)]
39. Bharath, G.; Anwer, S.; Mangalaraja, R.V.; Alhseinat, E.; Banat, F.; Ponpandian, N. Sunlight-Induced photochemical synthesis of Au nanodots on alpha-Fe₂O₃@Reduced graphene oxide nanocomposite and their enhanced heterogeneous catalytic properties. *Sci. Rep.* **2018**, *8*, 5718. [[CrossRef](#)]
40. Li, X.; Shen, R.; Ma, S.; Chen, X.; Xie, J. Graphene-based heterojunction photocatalysts. *Appl. Surf. Sci.* **2018**, *430*, 53–107. [[CrossRef](#)]
41. Shi, L.; Ma, J.; Yao, L.; Cui, L.; Qi, W. Enhanced photocatalytic activity of Bi₁₂O₁₇C₁₂ nano-sheets via surface modification of carbon nanotubes as electron carriers. *J. Colloid Interface Sci.* **2018**, *519*, 1–10. [[CrossRef](#)]
42. Micheroni, D.; Lan, G.; Lin, W. Efficient electrocatalytic proton Reduction with carbon nanotube-supported metal-organic frameworks. *J. Am. Chem. Soc.* **2018**, *140*, 15591–15595. [[CrossRef](#)] [[PubMed](#)]
43. Wang, J.; Qin, C.; Wang, H.; Chu, M.; Zada, A.; Zhang, X.; Li, J.; Raziq, F.; Qu, Y.; Jing, L. Exceptional photocatalytic activities for CO₂ conversion on Al-O bridged g-C₃N₄/ α -Fe₂O₃ z-scheme nanocomposites and mechanism insight with isotopes. *Appl. Catal. B Environ.* **2018**, *221*, 459–466. [[CrossRef](#)]